Journal of Power Sources 182 (2008) 383–388

Contents lists available at ScienceDirect

Journal of Power Sources

journal homepage: www.elsevier.com/locate/jpowsour

Electrodeposition of manganese dioxide in three-dimensional poly(3,4-ethylenedioxythiophene)–poly(styrene sulfonic acid)–polyaniline for supercapacitor

Feng-Jiin Liu*

Department of Chemical Engineering, National United University, 1 Lien Da, Kung-Ching Li, Miao-Li, Taiwan 36003

ARTICLE INFO

Article history:
Received 21 November 2007
Received in revised form 2 April 2008
Accepted 2 April 2008
Available online 10 April 2008

Keywords:
Poly(3,4-ethylenedioxythiophene)–poly(styrene sulfonic acid)–polyaniline
Manganese dioxide
Composite electrodes
Supercapacitors
Electrodeposition

ABSTRACT

The preparation of composites of precise metal oxides/conducting polymers is important in studies of supercapacitors. In this work, a three-dimensional matrix of poly(3,4-ethylenedioxythiophene)–poly(styrene sulfonic acid)–polyaniline (PEDOT–PSS–PANI) was prepared by interfacial polymerization of ANI into PEDOT–PSS. Conductivity was enhanced by incorporating of PANI into PEDOT–PSS because of the decrease in the distance for electron shuttling along the conjugated polymeric chain. Composite electrodes were prepared by the electrodeposition of manganese dioxide (MnO_2) in a PEDOT–PSS–PANI three-dimensional matrix. The electrodes were characterized by field emission scanning electron microscopy (FE-SEM), X-ray photoelectron spectroscopy (XPS), and cyclic voltammetry techniques. The results show a significant improvement in the specific capacitance of the composite electrode. For PEDOT–PSS the specific capacitance was of 0.23 F g^{-1}, while PEDOT–PSS–PANI and PEDOT–PSS–PANI–MnO_2 displayed values of 6.7 and 61.5 F g^{-1}, respectively. When only considering the MnO_2 mass, the composite had the specific capacitance of 372 F g^{-1}. The composite also had an excellent cyclic performance.

1. Introduction

Growing demands for the generation of power sources with transient high-power density have stimulated great interest in electrochemical capacitors in recent years [1,2]. Electrochemical capacitors are basically classified into two types depending on the nature of the charge-storage mechanism [3], the electric double layer capacitor and the electrochemical pseudocapacitor.

The electrodes of electrochemical redox supercapacitors consist of electroactive materials with several oxidation states. These types of capacitors have been extensively investigated in the recent times because of their high capacitative and energy characteristics [4,5]. Since the pseudocapacitance comes from the reversible redox transitions of the electroactive materials, transition metal oxides [6-8] and conducting polymers [9,10] with various oxidation states are regard as promising materials for the application in redox supercapacitors. Of the various transition metal oxide materials that have been investigated over the years, hydrous RuO_2 exhibits promising properties as a pseudocapacitor material [11,12]. Although RuO_2 is the material that presents the highest specific capacitance values (760 F g^{-1}), it has the inherent disadvantage of being both expensive and toxic. Nowadays, most research on electrochemical capacitors aim to increase power and energy densities as well as lower fabrication costs while using environment-friendly materials. So there is an increasing interest in the development of composite electrodes combined with conducting polymers and metal oxides.

In view of finding an inexpensive alternate to RuO_2, hydrous manganese oxide has recently been prepared by both chemically and electrochemically, and it was found to possess capacitive characteristics with acceptable values of specific capacitance [13,14]. Conducting polymers such as polyaniline (PANI) [15], polypyrrole (PPY) [16], and poly(3,4-ethylenedioxythiophene)–poly(styrene sulfonic acid) (PEDOT–PSS) [17] are promising matrix materials for embedding metal and metal oxide particles for application in electronic devices. Thus, we expect that a composite material, MnO_2 deposited on PANI, can be obtained by a potentiostatic deposition for high performance redox capacitors. Hu and Tsou [18] reported that MnO_2 exhibits the better electrochemical performance in 0.1 M Na_2SO_4 (neutral) than in 0.5 M H_2SO_4 (acid) solution. However, pristine PANI normally looses its electrochemical activity as the pH is raised from acidic to neutral conditions [19]. Modification of electrode surfaces provides an attractive way for overcoming this problem.

* Tel.: +886 37 381572; fax: +886 37 332397.
E-mail address: liu@nuu.edu.tw.

0378-7753/$ – see front matter © 2008 Elsevier B.V. All rights reserved.
doi:10.1016/j.jpowsour.2008.04.008

PEDOT doped with an excess of PSS, designated as PEDOT–PSS, is commercially available as a stable aqueous dispersion. Ghosh and Inganas [20] reported that PEDOT–PSS is a non-stoichiometric polyelectrolyte complex of PEDOT and PSS, with an excess of the latter component. The excess of SO_3H groups in PEDOT–PSS act as a nucleation site for PANI formation. The incorporating of PANI into PEDOT–PSS might decrease the distance for electrons hopping and lead to increase conductivity during the electrochemical reaction. Furthermore, the presence of SO_3H groups in PEDOT–PSS is essential for improving the electroactivity of PANI in a neutral electrolyte due to the "doping effect" of incorporating PSS. This served as motivating factor for investigating the feasibility of the preparation of PEDOT–PSS–PANI as supporting matrix for MnO_2 in supercapacitor application. In this work, studies on the preparation of MnO_2 using electrodeposition in a PEDOT–PSS–PANI matrix are reported on. The electrochemical performances of PEDOT–PSS, PEDOT–PSS–PANI, and PEDOT–PSS–PANI–MnO_2 composite electrodes for supercapacitors were investigated. The composite electrode materials are expected to greatly improve the performance of the supercapacitors leading to higher energy and power capability for various applications.

2. Experimental

2.1. Chemicals

Reagent grade aniline (ANI) (Merck) was doubly distilled and the resulting colorless liquid was kept in dark at 5 °C. PEDOT–PSS (Baytron P, VPCH8000, Bayer) was used without any further treatment. All solutions were prepared from double distilled water and $MnSO_4$ (Aldrich), sulfuric sodium (Merck) were used as received.

2.2. Preparation of PEDOT–PSS–PANI

A solution of ANI (0.5 mmol) was prepared in chloroform (10 mL). 10 mL of 0.125 mmol APS was prepared in PEDOT–PSS. These two solutions were mixed. The aniline/chloroform solution formed the lower organic layer and the Pt precursor-PSS solution formed the upper aqueous layer. The resulting two-phase system was covered with stretched parafilm to minimize solvent evaporation and was left undisturbed for ~12 h. After ~12 h, the reaction mixture was suction filtered and the dark black precipitate was washed repeatedly with double distilled water and acetone, until the filtrate become colorless.

2.3. Electrodeposition of MnO_2

PEDOT–PSS/PEDOT–PSS–PANI matrix electrodes were prepared by spin coating (2000 rpm for 1 min) on an indium tin oxide (ITO) substrate. The loading of the PEDOT–PSS/PEDOT–PSS–PANI was the weight difference of the bare ITO and after PEDOT–PSS/PEDOT–PSS–PANI coating. The MnO_2 was deposited on PEDOT–PSS/PEDOT–PSS–PANI electrodes by anodic deposition. The plating solutions, consisting of 0.25 M $MnSO_4$ with pH 6.5, were stirred on a hot plate during the deposition process. The deposition was performed at 0.75 V with a total passed charge of 0.1 C cm^{-2}. After the deposition of MnO_2 into PEDOT–PSS/PEDOT–PSS–PANI films, the electrodes were rinsed with double distilled water for 5 min and then dried at 150 °C for 30 min.

2.4. Physical and electrochemical characterizations

Resistance calculations were obtained was based on voltage/current characteristics measured with PGSTAT20 electrochemical analyzer, AUTOLAB Electrochemical Instrument (The Netherlands). Samples for these measurements were deposited onto glass substrates. The substrates with the deposited materials were contacted to the electrometer by means of silver wires and silver paint. The surface morphology of PEDOT–PSS, PEDOT–PSS–PANI, and PEDOT–PSS–PANI–MnO_2 was observed using scanning electron microscopy (SEM) (Philips X1-40 FEG). The X-ray photoelectron spectroscopy (XPS) measurement was performed with ESCA 210 and MICROLAB 310 D (VG Science Ltd., U.K.) spectrometers.

Electrochemical characterization was performed with PGSTAT20 electrochemical analyzer, AUTOLAB Electrochemical Instrument (The Netherlands). All experiments were carried out in a three-component cell. ITO coated glass plate (1 cm^2 area), Ag/AgCl (in 3 M KCl) and platinum wire were taken as working, reference, and counter electrodes, respectively. A Luggin capillary, whose tip was set a distance of 1–2 mm from the surface of the working electrode, was used to minimize errors due to ionic resistance (iR) drop in the electrolytes.

3. Results and discussion

The enhancement of conductance for incorporating PANI into PEDOT–PSS was studied using current/voltage (I/V) measurement. Fig. 1 illustrates the I/V characteristics of PEDOT–PSS and PEDOT–PSS–PANI. The linear behavior highlighted the ohmic properties of the materials, which allowed the evaluation of the related resistance by applying Ohm's first law ($R = V/I$). The calculation resistance is 9.13×10^8 and 6.12×10^6 Ω for PEDOT–PSS and PEDOT–PSS–PANI, respectively. The experimental data obtained from the calculation highlighted the enhancement of the conductivity when incorporating PANI into PEDOT–PSS. The incorporation of PANI into PEDOT–PSS plays an important role for improving the conductivity of PEDOT–PSS. A model picture representing the possible incorporation of PANI into PEDOT–PSS to enhance the conductivity of PEDOT–PSS is shown in Fig. 2. PEDOT–PSS are the stable aqueous dispersion colloidal particles due to the excess of PSS component in PEDOT–PSS [20]. However, PSS is a noncondcutive material. The excess of PSS component in PEDOT–PSS can increase the distance for electron shuttling along the PEDOT

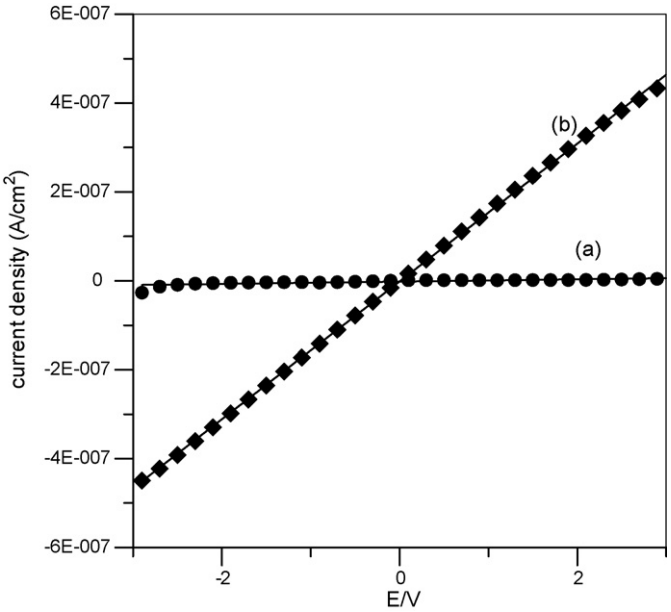

Fig. 1. I/V characteristics of (a) PEDOT–PSS and (b) PEDOT–PSS–PANI.

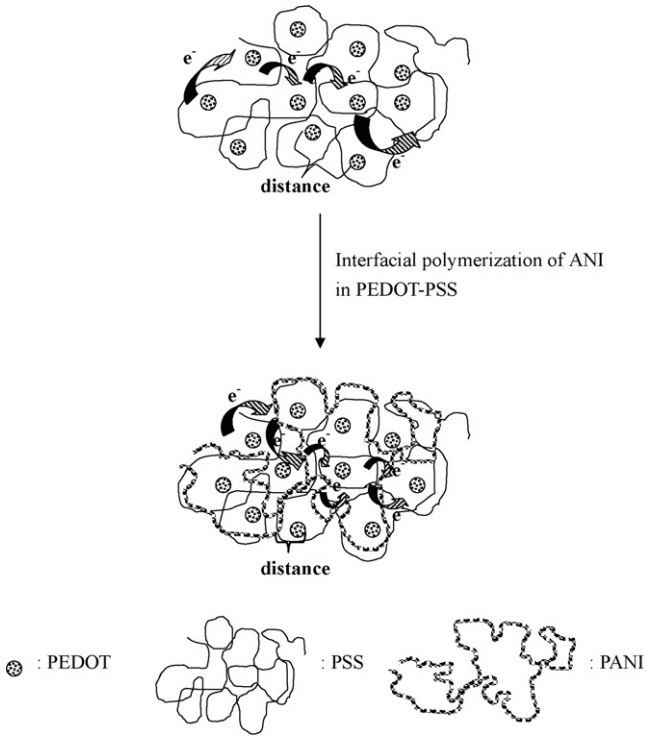

Fig. 2. Helping the incorporation of PANI into PEDOT–PSS for shuttling electrons through the conjugation polymer chain.

conjugated chain (Fig. 2a). Hence, the interfacial synthesis method is employed to incorporate an additional conjugated polymer (PANI) into PEDOT–PSS for improving its conductivity. The excess PSS acts as the template for PANI formation into PEDOT–PSS. In the present case, ANI moieties are statically aligned at the interface by the interacting with the anionic polymer electrolyte (PSS). The SO_3H groups are expected to be preferentially oriented in the upper layer of aqueous phase. However, the basic nature of ANI moieties prefers orientation with the SO_3H groups at the interface. Thus, the ANI moieties are aligned over the backbone of PSS in an ordered fashion. Upon polymerization, these ordered ANI molecules are polymerized along the backbone of PSS. The insertion of PANI conjugated chain between the PEDOT colloids can reduce the distance for electron shuttling and lead to the improvement of conductivity for PEDOT–PSS–PANI.

The SEM images of PEDOT–PSS, PEDOT–PSS–PANI, and PEDOT–PSS–PANI–MnO_2 are shown in Fig. 3. The morphology of PEDOT–PSS (Fig. 3a) shows a compact and porous structure. Interestingly, a rod-like structure can be obtained by incorporating PANI into PEDOT–PSS (Fig. 3b), implying the successful incorporation of PANI into PEDOT–PSS matrix. The dramatic change in morphology (Fig. 3c) can be observed when MnO_2 is deposited in PEDOT–PSS–PANI matrix. As can be seen from the figure, the PEDOT–PSS–PANI rods look as if they are completely covered by spherical MnO_2 nanoparticles (in nano size), and forming rod-of-beads structure. Spherical MnO_2 particles in nano size on polymer lead to more sites that are susceptible to redox reaction, a greater active area and, consequently, higher capacitance.

The XPS spectrum of PEDOT–PSS–PANI–MnO_2 is shown in Fig. 4. From the observation of the survey scan of PEDOT–PSS–PANI–MnO_2, the existence of Mn 3p and Mn 2p signals supplied clear evidence that MnO_2 particles had been successfully embedded in PEDOT–PSS–PANI matrix. The Mn 2p region consisted of a spin-orbit doublet with Mn $2p_{1/2}$ having a binding energy of 653.5 eV and Mn $2p_{3/2}$ with a binding energy of

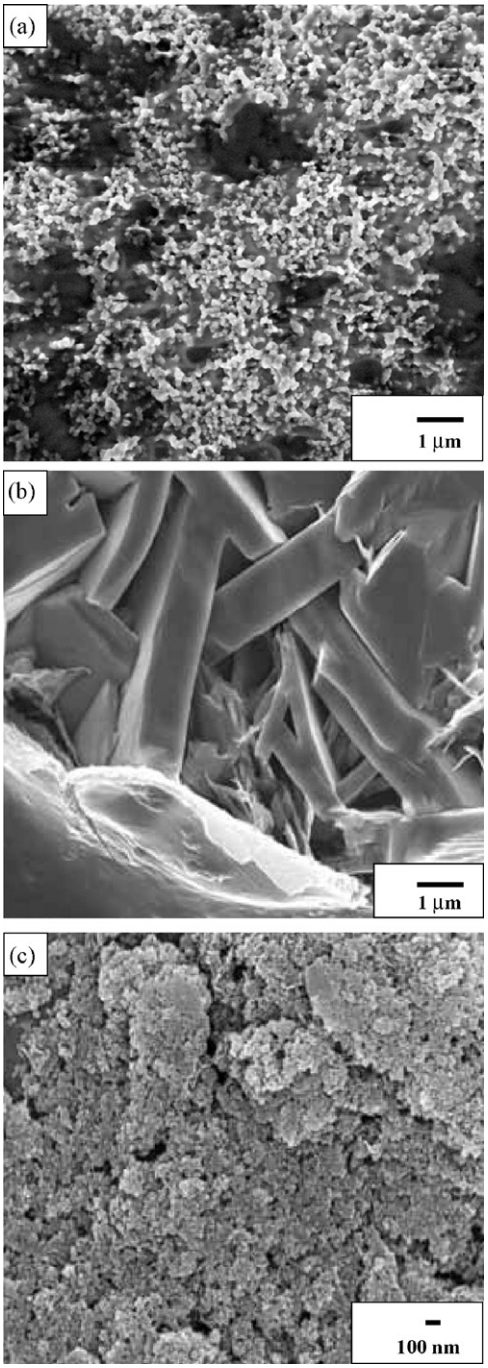

Fig. 3. FE-SEM images of (a) PEDOT–PSS, (b) PEDOT–PSS–PANI, and (c) PEDOT–PSS–PANI–MnO_2.

641.5 eV, which are characteristic of a mixed-valence manganese system (Mn^{4+} and Mn^{3+}) [21]. The O 1s spectrum was analyzed by curve fitting according to Toupin and co-workers [22]. The spectrum can be fitted with three components respectively related to Mn—O—Mn bond (531.1 eV) for the tetravalent oxide, Mn—OH bond (532.4 eV) for a hydrated trivalent oxide, and H—O—H bond (533.8 eV) for residual water. The area ratios are 0.65, 0.28, and 0.07 for Mn—O—Mn, Mn—OH, and H—O—H, respectively. The dominated oxidation state of MnO_2 in PEDOT–PSS–PANI is tetravalent oxide. Also, the results show that the oxide is in a hydrated form, which is similar to the hydrated form oxide film prepared by electrochemical deposition [23].

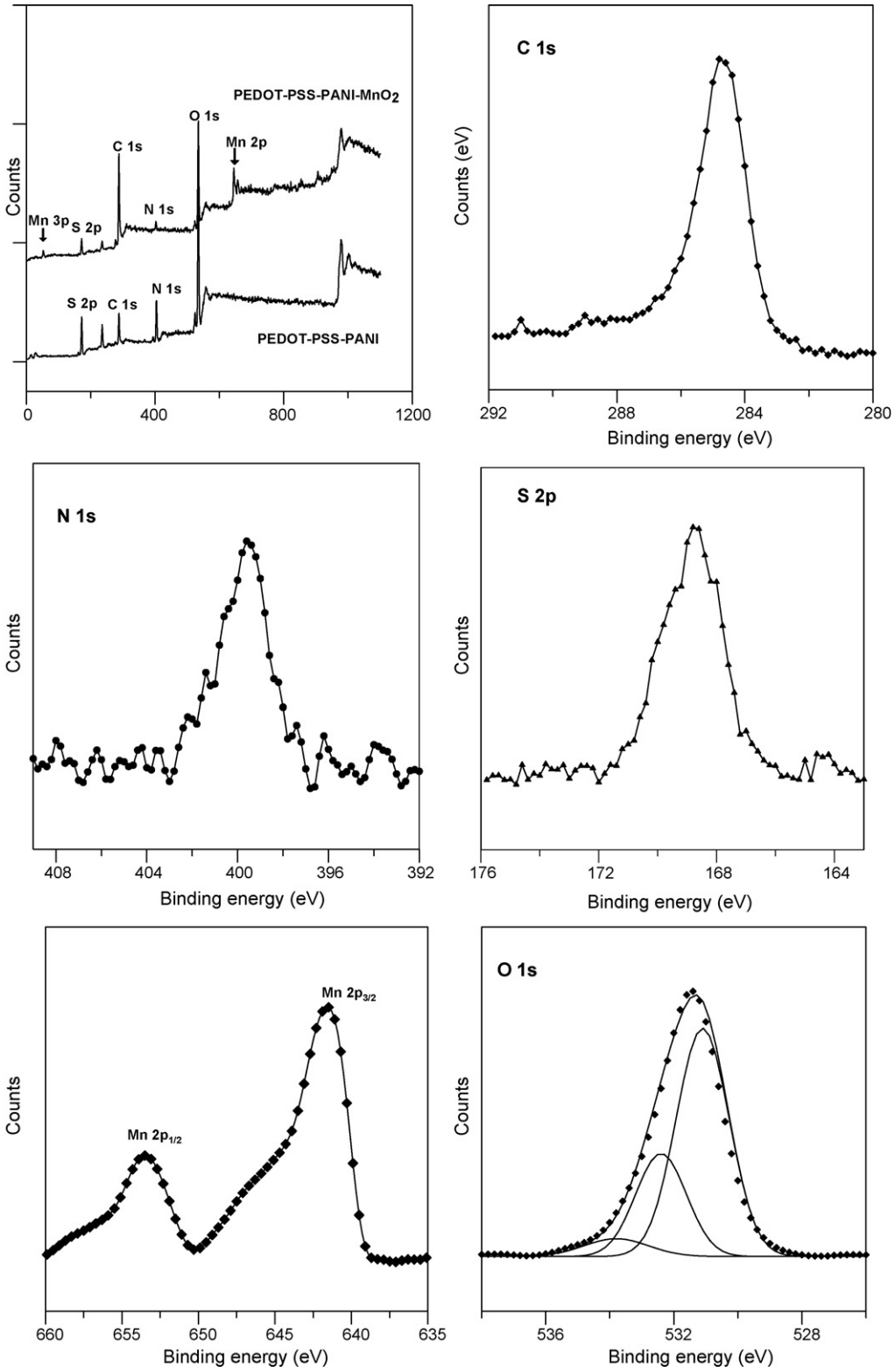

Fig. 4. XPS spectra of PEDOT–PSS–PANI–MnO_2.

Cyclic voltammetry (CV) was employed to evaluate the electrochemical capacitance performance of PEDOT–PSS, PEDOT–PSS–PANI, and PEDOT–PSS–PANI–MnO_2 composite electrodes in 0.1 M Na_2SO_4 solution as electrolyte. Fig. 5 shows the cyclic voltammograms for the electrodes recorded between 0.0 and 1.0 V. As seen in the voltammograms, the specific current of PEDOT–PSS–PANI (ca. 0.2 mA cm^{-2} g) is much higher than that of PEDOT–PSS (ca. 0.002 mA cm^{-2} g). The enhanced specific current for PEDOT–PSS–PANI can be attributed to the incorporation of PANI into PEDOT–PSS resulting in decreasing the distance for electron shuttling during the electrochemical reaction. As can be seen in Fig. 5, the dramatic change in specific current can be observed for

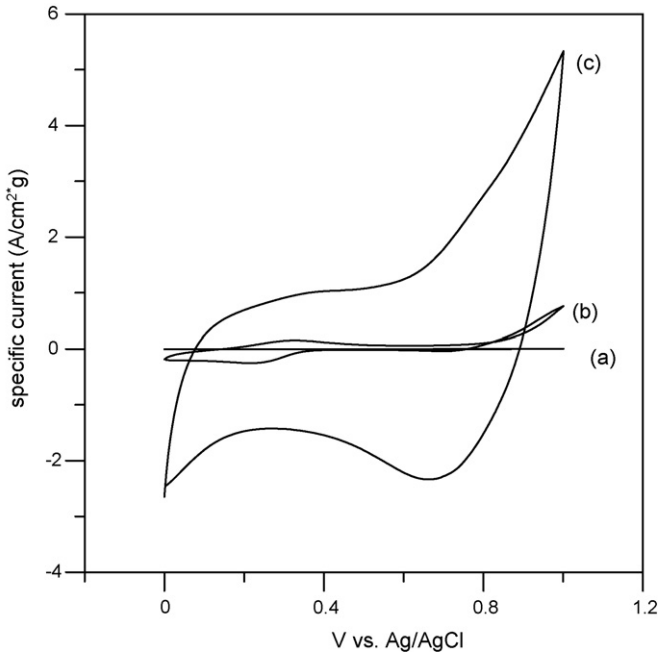

Fig. 5. Cyclic voltammetry of (a) PEDOT–PSS, (b) PEDOT–PSS–PANI, and (c) PEDOT–PSS–PANI–MnO_2 in 0.1 M Na_2SO_4 solution.

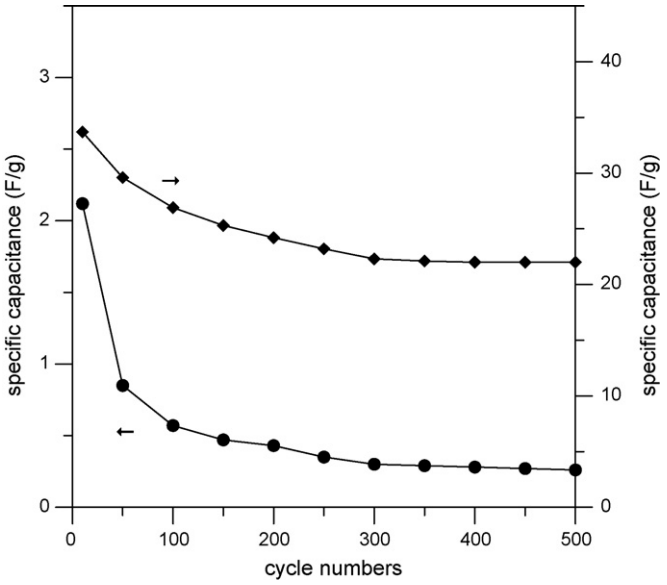

Fig. 6. Specific capacitance decay for (a) PANI–PEDOT–PSS and (b) PANI–PEDOT–PSS–MnO_2 composite electrodes in 0.5 M Na_2SO_4 against the cycle number of CV in the stability tests. Cyclic voltammograms were measured at 100 mV s^{-1} in 0.5 M Na_2SO_4.

MnO_2 particles deposited in PEDOT–PSS–PANI matrix. The specific capacitance of the electrodes can be estimated according to the following equation.

$$C = \frac{Q}{\Delta E m} \quad (1)$$

where C is the specific capacitance (F g^{-1}), Q is the voltammetric charge (C), ΔE is the potential window, and m is the mass of material (g).

The specific capacitance is 0.02, 6.67, and 61.5 F g^{-1} for PEDOT–PSS, PDOT–PSS–PANI, and PEDOT–PSS–PANI–MnO_2, respectively. The specific capacitance of PEDOT–PSS–PANI–MnO_2 is 9.2 times higher than the specific capacitance of PEDOT–PSS–PANI. It is important to point out that both PEDOT–PSS and PANI are also capacitive materials. However, as seen in Fig. 5, the specific current of PEDOT–PSS and PEDOT–PSS–PANI in Na_2SO_4 electrolyte is much smaller than the MnO_2 deposits. After subtracting the contribution of PEDOT–PSS–PANI host, a high pseudocapacitance of about 372 F g^{-1} for the MnO_2 was calculated. PEDOT–PSS–PANI does not contribute significantly to the total capacitance of the electrode due to the low electroactivity of PEDOT–PSS and PANI in aqueous Na_2SO_4 solution (neutral) as electrolyte [24,19]. Nevertheless, its presence helps MnO_2 particles to disperse over a large area, thereby increasing the active surface are of MnO_2. Furthermore, the incorporation of PANI into PEDOT–PSS provides a low resistance path within the electrode, and the existence of SO_3H groups in PSS generates a pathway for protonic species that increase the ionic conductivity [25].

The stability of electrodes was performed by subjecting PEDOT–PSS–PANI and PEDOT–PSS–PANI–MnO_2 electrodes for longer number of cyclic voltammetric scans. The cyclic was performed at a scan rate of 100 mV s^{-1} for 500 cycles. Fig. 6 shows the variation of specific capacitance as a function of cycle number. It is obvious that the loss of specific capacitance for PEDOT–PSS–PANI is larger; in contrast, the loss of specific capacitance for PEDOT–PSS–PANI–MnO_2 composite electrode is smaller and shows a stable cycle life in the potential of 0–1.0 V, capacitance retention of about 68% was found over 500 cycles. Such a low decrease in specific capacitance after long time operation indicates the high stability of the composite and its potential as an electrode material for long-term capacitor applications. Based on the above results, the introduction of MnO_2 particles into PEDOT–PSS–PANI matrix can promote the capacitance, stability and the cycle life of the composite electrodes.

4. Conclusion

Through a simple design, the incorporation of PANI into PEDOT–PSS matrix was achieved using an interfacial synthesis route. The incorporation of PANI in PEDOT–PSS provides an extra path way for electron shuttling along the conjugated polymer chain and lead to an enhancement of conductivity. MnO_2 particles could be electrochemically embedded in to conductive PEDOT–PSS–PANI matrix. The CV studies showed that PEDOT–PSS–PANI–MnO_2 exhibit a higher capacitance than PEDOT–PSS and PEDOT–PSS–PANI. The conductive matrix, PEDOT–PSS–PANI, provides an improvement in conductivity for electron transporting during the electrochemical reaction and a suitable environment for dispersing MnO_2 particles without aggregation, evident from the SEM results. Also, the pending sulfonic acid groups on PSS provide a pathway for proton migration. PEDOT–PSS–PANI–MnO_2 composite has the essential characteristics for a super capacitor electrode.

Acknowledgement

The authors wish to thank the National Science Council in Taiwan for financial support of this work (grant number NSC 95-2622-E-239-009-CC3).

References

[1] M. Jayalakshmi, M.M. Rao, J. Power Sources 157 (2006) 624.
[2] N.L. Wu, S.Y. Wang, C.Y. Han, D.S. Wu, L.R. Shiue, J. Power Sources 113 (2003) 173.
[3] B.E. Conway, J. Electrochem. Soc. 138 (1991) 1539.
[4] Z.J. Lao, L. Konstantino, Y. Tournaire, S.H. Ng, G.X. Wang, H.L. Liu, J. Power Sources 162 (2006) 1451.

[5] E. Frackowiak, V. Khomenko, K. Jurewicz, K. Lota, F. Benguin, J. Power Sources 153 (2006) 413.
[6] A.V. Rosario, L.O.S. Bulhoes, E.C. Pereira, J. Power Sources 158 (2006) 795.
[7] E. Machefaux, T. Brousse, D. Belanger, D. Guyomard, J. Power Sources 165 (2007) 651.
[8] C.C. Hu, M.J. Liu, K.H. Chang, J. Power Sources 163 (2006) 1126.
[9] M.D. Ingram, H. Staesche, K.S. Ryder, J. Power Sources 129 (2004) 107.
[10] C.P. Fonseca, J.E. Benedetti, S. Neves, J. Power Sources 158 (2006) 789.
[11] Y.T. Kim, K. Tadai, T. Mitani, J. Mater. Chem. 15 (2005) 4914.
[12] M.S. Dandekar, G. Arabale, K. Vijamohanan, J. Power Sources 141 (2005) 198.
[13] R.N. Reddy, R.G. Reddy, J. Power Sources 132 (2004) 526.
[14] K.R. Prasad, N. Miura, J. Power Sources 135 (2004) 354.
[15] L.M. Huang, W.R. Tang, T.C. Wen, J. Power Sources 164 (2007) 526.
[16] J.W. Lee, B.N. Popov, J. Power Sources 161 (2006) 565.
[17] L.M. Huang, T.C. Wen, A. Gopalan, Electrochim. Acta 51 (2006) 3469.
[18] C.C. Hu, T.W. Tsou, Electrochem. Commun. 4 (2002) 105.
[19] G. Milczarek, Electrochem. Commun. 9 (2007) 123.
[20] S. Ghosh, O. Inganas, Adv. Mater. 11 (1999) 1214.
[21] M. Chigane, M. Ishikawa, J. Electrochem. Soc. 147 (2000) 2246.
[22] T. Brousse, M. Toupin, D. Bélanger, J. Electrochem. Soc. 151 (2004) A614.
[23] J.-K. Chang, W.-T. Tsai, J. Electrochem. Soc. 150 (2003) A1333.
[24] A.K.C. Gallegos, M.E. Rincon, J. Power Sources 162 (2006) 743.
[25] C.W. Kuo, L.M. Huang, T.C. Wen, A. Gopalan, J. Power Sources 160 (2006) 65.